Elastic and inelastic scattering of uranium ions by holmium, gold, and bismuth targets

H. A. Khan and I. E. Qureshi

Nuclear Engineering Division, Pakistan Institute of Nuclear Science and Technology (PINSTECH), Nilore, Rawalpindi, Pakistan

W. Westmeier and R. Brandt

Kernchemie, Philipps-Universität, D-3550 Marburg, Federal Republic of Germany

P. A. Gottschalk

Gesellschaft für Reaktorsicherheit (GRS)mbH, D-5000 Köln, Federal Republic of Germany

Angular distributions for elastic scattering of ^{238}U ions by ^{165}Ho, ^{197}Au, and ^{209}Bi at 2380 MeV have been obtained in a 2π geometry using solid state nuclear track detectors. The angular distributions of the elastic differential cross section ratios $\sigma_{el}(\text{expt.})/\sigma(\text{Ruth})$ are analyzed using (a) the generalized Fresnel model and (b) the parametrized S-matrix method. Quarter-point angles obtained are converted to reaction parameters such as grazing angular momenta, interaction radii, and total reaction cross sections. Values of inelastic total reaction cross sections were obtained by directly counting the three-, four-, and five-prong events along with the two-prong inelastic events as observed in the 2π geometry. Experimental total reaction cross sections are compared with optical and sharp cutoff model calculations. There is good agreement among the total reaction cross sections evaluated from elastic and inelastic data as well as with model calculations.

I. INTRODUCTION

Most of the charged particle interaction studies carried out in the past employed light projectiles. With the availability of heavier projectiles, interest in heavy-projectile heavy-target systems has increased. This is basically due to the fact that heavy systems show the existence of new modes of interaction, in particular the so-called deep inelastic interaction.[1-5] A rather detailed review has been published by Schröder and Huizenga.[6] The observation of this new mode is particularly significant in experiments performed with projectiles heavier than argon in combination with heavy targets.[7,8] In order to determine the partial cross sections of different modes of interaction, and to ensure that all possible exit channels have been identified, unambiguous determination of the experimental total reaction cross section is of prime importance.[9,10]

A number of experiments have been carried out to obtain the total reaction cross sections of heavy projectiles with heavy targets.[11-13] Attempts have been made for the correlation of the already existing data, and improved determinations of reaction parameters.[14,15] Optical and strong-absorption models have been used along with the data obtained from elastic scattering from heavy systems for the determination of total reaction cross sections.[16,17] According to Frahn,[18] an analytical expression for the angular distribution in elastic scattering can be obtained from the Fresnel scattering model.[19] Blair[20] has shown that the quarter-point angle can be employed for the determination of the total reaction cross section and other reaction parameters. An unambiguous determination of the total reaction cross section can be obtained by an exclusive measurement of all reaction products.

This paper describes the use of mica solid state nuclear track detectors (SSNTD) in a 2π geometry[21,22] for the study of elastically scattered ^{238}U ions by heavy targets of ^{165}Ho, ^{197}Au, and ^{209}Bi. The experimental data are analyzed using the generalized Fresnel model[23] and the parametrized S-matrix method.[24] Total reaction cross sections and other reaction parameters are deduced. Experimental values of the total reaction cross section are also obtained from the study of two-prong inelastic and multiple-prong (particularly, three-, four-, and five-prong) events, produced in mica track detectors. These values are compared with theoretical reaction cross sections from the optical model and the sharp cutoff approximation.

A comparison of the experimental and theoretical total inelastic reaction cross sections and those deduced from elastic scattering using the generalized Fresnel model and the parametrized S-matrix method is made.

II. EXPERIMENTAL DETAILS AND METHOD

Details of the 2π-geometry technique have already been published (Refs. 4, 21, and 22). These calibration experiments show that if Muscovite mica is used in 2π geometry, all charged particles having masses > 30 u, and scattered into the forward hemisphere ($\theta_{lab} < 85°$) are registered.

Thin targets (≈ 1 mg/cm^2) of gold, holmium, and bismuth were vacuum deposited on freshly cleaved Muscovite mica sheets. The target-detector combinations (target upstream) were exposed perpendicularly to ^{238}U ions of 10 MeV/u, obtained from the UNILAC (GSI, Darmstadt, West Germany). Before irradiation, the exposure conditions were optimized by measuring the charged

particle fluence with glass track detectors. The glass detectors were exposed under the same conditions and consecutively etched in 48% HF. The track densities obtained on these detectors directly yielded the fluence. It has been observed that, for the ease in track counting and in the analysis of the events, the optimum charged particle fluence is of the order of 10^6 particles/cm^2. All exposures for the present studies were carried out according to these optimized exposure conditions. The target layers on the exposed detectors were removed by dissolving them in aqua regia or HNO$_3$. The mica detectors were then etched in 48% HF for 15 min at room temperature in order to reveal all latent damage trails due to different reaction products. The etching conditions had been previously optimized so as to etch the latent damages from all reaction products of an event up to their full length. An optical microscope coupled with a tracing tube and a depth measuring system was used for the analysis.

Values of the fluence received by the individual targets were obtained by counting the round (dot-like) etch pits produced by the projectiles on the mica detectors (see Fig. 2 in Ref. 4) and correcting for a few overlapping tracks. A large number of tracks were counted in order to achieve good counting statistics. Extrapolating the results to the total target area and taking into account the statistical errors induced by the finite areas investigated and possible inhomogeneities of the flux, we determined the total projectile flux within 6% uncertainty. Target thicknesses were obtained within 7% by weighting the mica detectors before and after removing the target layers from the detectors.

Special attention was paid to the analysis of two-prong events. Track lengths and track angles of correlated events were measured event by event. The track lengths could be determined within ±1.5 μm (standard deviation) for the bulk of the data. The uncertainties in track angles are ±2° (standard deviation). All binary events with angles $\alpha > 170°$ as seen in the plane perpendicular to the beam have been interpreted as genuine two-pronged events.

The track parameters (track length and their angles with respect to the original direction of the beam) of the two-prong events were converted to particle parameters (velocity, mass, energy, and scattering angle) assuming that the projected angle between both tracks of a two-pronged event (in the plane perpendicular to the beam) equals 180°. The data thus obtained were plotted in a track length (or velocity of the particles) versus scattering angle diagram. A theoretical curve for track length (or particle velocity) versus the scattering angle was obtained using the empirical[4] range-energy relationship in mica and the elastic scattering equation:[25]

$$V(l,A) = \sum_{\mu=0}^{2} \sum_{\nu=0}^{4} C_{\mu\nu} A^{\mu} l^{\nu}, \tag{1}$$

$$E_p = E_{\text{lab}} \frac{A_p^2}{(A_p + A_t)^2}$$

$$\times \left\{ \cos\theta_p \pm \left[\left(\frac{A_t}{A_p} \right)^2 - \sin^2\theta_p \right]^{1/2} \right\}^2, \tag{2}$$

where the symbols have the following meaning: V is the velocity of the reaction product (fm/10^{-23} s); A is the mass number of the recoiling atom; l is the range (mg/cm^2) of the particle in mica; $C_{\mu\nu}$ are the coefficients obtained from an empirical velocity-range relationship (see Ref. 4); E_p is the energy of the scattering projectile (laboratory); E_{lab} is the initial energy of the projectile in the laboratory system; A_p, A_t are the masses of the projectile and the target, respectively; θ_p is the scattering angle of the projectile (laboratory).

Values of the coefficients $C_{\mu\nu}$ were obtained from an empirical velocity-range calibration in muscovite mica for the particular batch used in the present experiment. These values are identical to those used by Gottschalk et al. (see Ref. 4). It is worth mentioning that the applicability of Eq. (1) is restricted to $30 < A < 260$ and $0.5 < l < 22$, and it is important to determine the coefficients empirically for each particular batch of track detecting material employed in the studies.

In order to separate elastic and inelastic events we proceed as follows: The (relative) uncertainties in determining the energies of two-pronged events are of the order of 4.5% and the mass resolution for individual two-pronged masses is known to be about 7% (see, e.g., Ref. 4). These values could be confirmed by the present experiment. Events lying on the theoretical elastic curve (within the energy and mass resolution of 4.5% and 7%, respectively) were thus taken as being due to "elastic" scattering and counted in 2° (c.m.) wide angular bins.

III. RESULTS AND DISCUSSION

A. Elastic events

The experimentally obtained ratios of elastic to Rutherford cross sections, $\sigma_{\text{scat}}(\text{expt.})/\sigma_{\text{scat}}(\text{Ruth})$ for ^{238}U on ^{165}Ho, ^{197}Au, and ^{209}Bi at 2380 MeV, are shown in Figs. 1–3. The error bars include the statistical uncertainties only. Actual errors are expected to be larger as some quasielastic events having little or no mass transfer may be included in the data. Systematic errors thus induced by the low resolution will be elaborated later on in more detail. The experimental cross section ratios $\sigma_{\text{scat}}(\text{expt.})/\sigma_{\text{scat}}(\text{Ruth})$ are based on absolute cross sections measured by counting the "elastic" events—as defined above—within appropriate angular bins and relating these events to the total projectile flux and target thickness.

The experimental points from all three sets of measurements (Figs. 1–3) show truncations in the angular distribution at forward angles. The main reason behind this truncation effect is a limitation of our measuring technique. The reaction products scattered in the very forward direction ($\theta_{\text{c.m.}} \lesssim 25°$) produce etched channels whose projected ranges are much shorter than those scattered at larger angles. The identification of such events as elastically scattered ones is difficult, and they may be either missed or are analyzed with low accuracy. The seriousness of this effect increases with decreasing scattering angle. However, since in the present studies we are primarily interested in angular distributions near the quarter point angle, the above-mentioned limitation of the
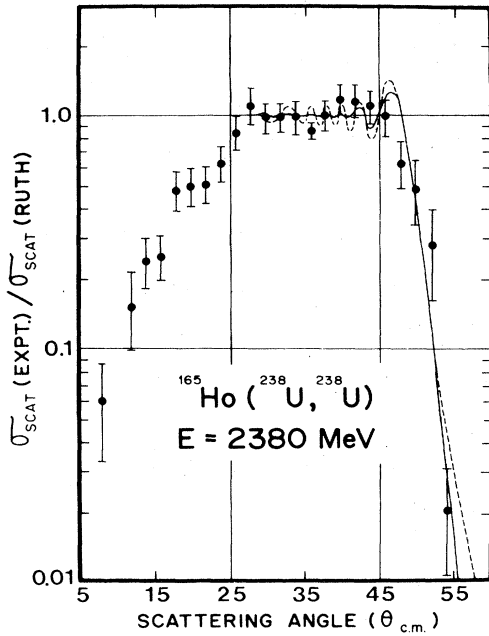
FIG. 1. Variation of the ratio of the experimental elastic scattering cross section to the Rutherford cross section as a function of scattering angle in the c.m. system for the ^{165}Ho+^{238}U reaction for ^{238}U projectile energy of 2380 MeV (laboratory system). The filled circles are experimental points and the error bars represent the statistical errors only. The dashed curve is for $\Delta=0$ in the χ^2 fitting of the generalized Fresnel model to the experimental data. The solid curve is for $\Delta=5.9$.
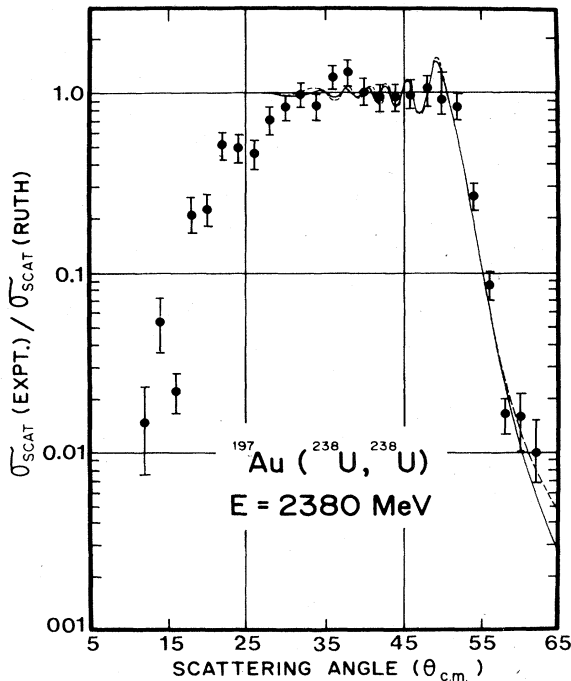
FIG. 2. Same as for Fig. 1 except that the target is ^{197}Au. The solid curve is for $\Delta=2.1$.
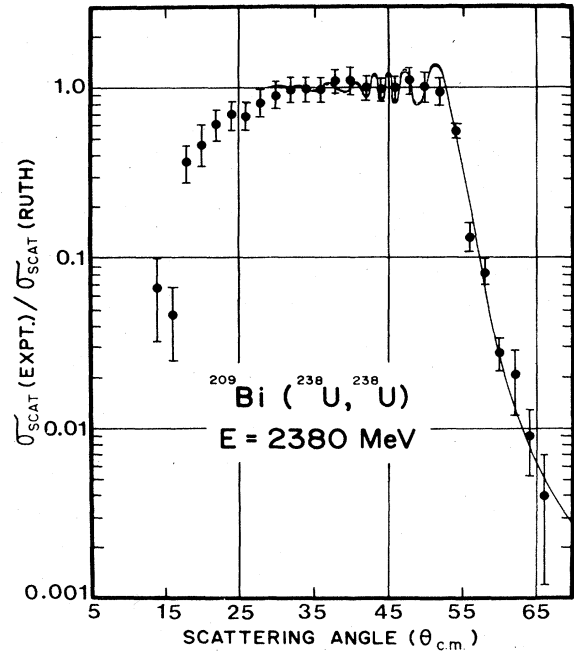
FIG. 3. Same as for Fig. 1 except that the target is ^{209}Bi. The solid curve is for $\Delta=0.7$.

SSNTD method does not significantly affect the measurements.

The experimental results of U + Ho,Au,Bi have been analyzed by using two different models: (a) the generalized Fresnel model, and (b) the parametrized S-matrix method.

1. Generalized Fresnel model (GFM)

According to the generalized Fresnel model,[23] the ratio σ_{el}(expt.)/σ(Ruth) is fitted by the equation

$$\frac{\sigma_{el}}{\sigma_{Ruth}}=1+\tfrac{1}{2}[(\tfrac{1}{2}-C)^2+(\tfrac{1}{2}-S)^2]F^2+F(C+S-1),$$
$$\theta\leq\theta_{1/4}\quad(3)$$
$$=\tfrac{1}{2}[(\tfrac{1}{2}-C)^2+(\tfrac{1}{2}-S)^2]F^2,\qquad\theta>\theta_{1/4}$$

where $C\equiv C(\,|x\,|\,)$ and $S\equiv S(\,|x\,|\,)$ are the real and imaginary parts of the Fresnel integral, respectively. The explicit form of the function $F(y)$ can be written as

$$F(y)=\pi y/\sinh\pi y \ . \tag{4}$$

The arguments x and y are related to the quarter point angle $\theta_{1/4}$ and the l-space window parameter Δ through equations

$$x=[\Lambda(\pi\sin\theta_{1/4})]^{1/2}(\theta-\theta_{1/4}) \ ,$$
$$y=\Delta(\theta_{1/4}-\theta) \ , \tag{5}$$

where Λ is the grazing angular momentum described as $\Lambda=\eta\cot(\tfrac{1}{2}\theta_{1/4})$, and η is the Sommerfeld parameter.

Detailed discussion of the above equations is given in Ref. 23.

The total elastic reaction cross section is given in terms of Λ and Δ as

$$\sigma_R = \frac{\pi\Lambda^2}{k^2}\left[1+\frac{2\Delta}{\Lambda}+\frac{\pi^2}{3}\left[\frac{\Delta}{\Lambda}\right]^2\right],\tag{6}$$

where k is the Fermi wave number.

For the reactions under study, a good fit to the elastic differential cross section ratios $\sigma_{el}/\sigma_{Ruth}$ is obtained by varying the parameters $\theta_{1/4}$ and Δ. The fitted values of the parameters are given in Table I where the fit refers to the angular range $\theta_{c.m.} > 30°$. The quoted errors result from the statistical uncertainties of the experimental data as well as the two-dimensional χ^2 fit. Using SSNTD techniques, the cross section for elastic events is subject to systematic uncertainties, as inelastic products with little or no net mass transfer and with low energy loss might erroneously be classified as "elastic." This will be discussed in Sec. III B.

The comparison of calculated angular distributions with the experimental values is shown in Figs. 1—3, where the distributions for $\Delta=0$ are plotted as dashed curves. Increasing the value of Δ, improves the slope of σ_{el}(expt.)/σ(Ruth) at angles $\theta > \theta_{1/4}$ (solid curves in Figs. 1—3). The shape of the curve near $\theta_{1/4}$ is largely determined by the fitted parameter $\theta_{1/4}$. The value of Δ affects the amplitudes of oscillations at small angles as well as the slope at $\theta > \theta_{1/4}$ (Ref. 23). Since there is an experimental bias for forward angles, these data points are not included in the fitting procedure.

2. Parametrized S-matrix method (PSM)

In the framework of Blair's cutoff approximation to elastic scattering[20] and with consideration of empirical phase shift terms[24] the ratio σ_{el}/σ(Ruth) is evaluated by the equation

$$\frac{\sigma_{el}}{\sigma_{Ruth}} = \left| -i\exp\{-i\eta\ln[\sin^2(\theta/2)]\} - \eta^{-1}\sin^2(\theta/2)\sum_{l=0}^{\infty}(1-S_l)(2l+1)P_l(\cos\theta)\exp[2i(\sigma_l-\sigma_0)]\right|^2,\tag{7}$$

where σ_l is the Coulomb phase shift. The nuclear scattering matrix

$$S_l = A_l\exp(2i\delta_l)\tag{8}$$

is parametrized using the phenomenological form for the reflection coefficient A_l and the nuclear phase shift δ_l. Following the smooth cutoff parametrization of McIntyre et al.[24] we have used

$$A_l = \left\{1+\exp\left[-\frac{(l+0.5)-\Lambda}{\Delta}\right]\right\}^{-1}\tag{9}$$

and

$$\delta_l = \delta_0\left\{1+\exp\left[-\frac{(l+0.5)-\Lambda}{\Delta}\right]\right\}^{-1}.\tag{10}$$

In the final analysis we used $\delta_0=0$ for the nuclear phase shift normalization parameter, since no improve-

ment in the fit was obtained with nonzero δ_0. The two parameters Λ and Δ of A_l were obtained by a χ^2 minimization procedure. The resulting analysis of the data from Figs. 1—3 is shown by solid lines in Fig. 4 where the dots are experimental data. Again, owing to the experimental bias in this region, part of the data that is at small angles is not used in the fitting. The values of Λ (and associated $\theta_{1/4}$) and Δ along with their uncertainties resulting from the statistical errors of the data and fitting procedure are also given in Table I with the overall χ^2 listed in the last column.

From the grazing angular momenta Λ obtained in the above two analyses, we calculate the interaction radius parameter r_0 as[23]

$$r_0(A_p^{1/3}+A_t^{1/3}) = \frac{(\Lambda^2+\eta^2)^{1/2}+\eta}{k}.\tag{11}$$

Again the uncertainties in r_0 pertain to the statistical er-

TABLE I. Parameters and statistical uncertainties deduced from elastic events.

Parameter	k (fm^{-1})	η	$\theta_{1/4}$ GFM	$\theta_{1/4}$ PSM	$\frac{1}{2}+lg=\Lambda$ ($\hbar$) GFM	PSM	Δ ($\hbar$) GFM	PSM	r_0 (fm) GFM	PSM	χ^2 GFM	PSM
Target (energy)												
^{165}Ho (2380 MeV)	67.4	307.0	50.7 ±0.8	50.9 ±0.9	647.4 ±11.5	649.8 ±13.9	5.9 ±1.5	6.4 ±1.7	1.300 ±0.014	1.304 ±0.015	0.35	0.34
^{197}Au (2380 MeV)	74.6	362.0	53.8 ±0.4	53.9 ±0.5	712.9 ±6.0	711.9 ±8.5	2.1 ±2.7	3.6 ±1.9	1.297 ±0.006	1.296 ±0.007	0.26	0.29
^{209}Bi (2380 MeV)	77.0	380.3	55.5 ±0.4	55.3 ±0.3	722.3 ±6.9	724.8 ±4.5	0.7 ±4.6	0.2 ±2.3	1.282 ±0.006	1.285 ±0.004	0.15	0.10
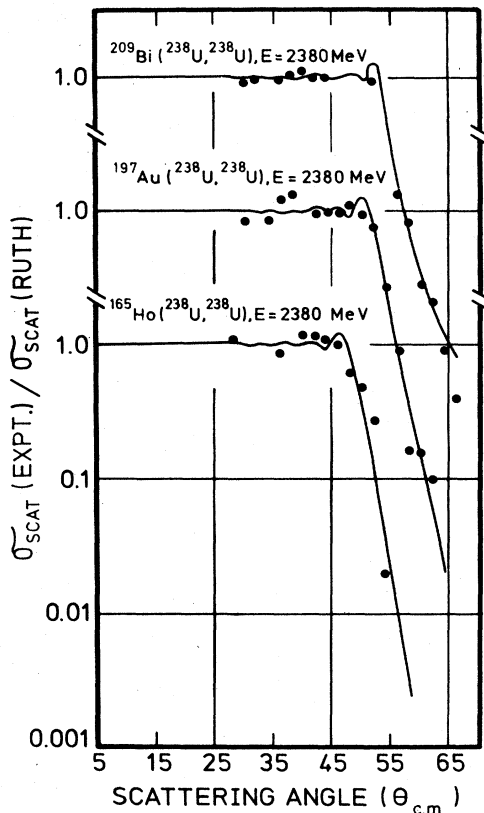
FIG. 4. Variation of the ratio of experimental elastic scattering to the Rutherford cross sections as a function of scattering angle in the c.m. system for the reaction of 2380 MeV ^{238}U ions with ^{165}Ho, ^{197}Au, and ^{209}Bi targets. The curves represent the χ^2 fits with the parametrized S-matrix method to the experimental points (full dots). Δ values of 6.4, 3.6, and 0.2, are used for ^{165}Ho, ^{197}Au, and ^{209}Bi, respectively.

rors of the data and the two-dimensional χ^2 fit. At the present level of uncertainties, the experimental data do not indicate variations of r_0 with the increasing combined mass $A_{CN} = (A_P + A_T)$ or increasing (center of mass) energy.

B. Inelastic events

An unambiguous determination of the experimental total reaction cross section can be obtained by an exclusive measurement of all inelastic reaction products. In the present work, experimental values for the total inelastic reaction cross section were obtained by adding the cross sections for three-, four-, and five-prong events, and for two-prong inelastic events. All multiprong events were scanned (on a total detector area of more than 90 cm^2 for each reaction) using a tracing system attached to the microscope. All multiprong events where the tracing did not show a common origin of the tracks and/or their orientation was not in the right direction were not included in the count. Tracks of non-nuclear origin (such as crystal defects, scratches, artifacts, etc.) were eliminated by visual inspection. The probability for an accidental overlap of two independent two-prong events resembling a four-

prong event is estimated to be less than 10^{-4} and corrections are thus neglected. The experimental total inelastic reaction cross sections counted for ^{165}Ho, ^{197}Au, and ^{209}Bi targets are listed in Table II. These are absolute cross sections as they have been obtained by counting the inelastic reaction products and relating this number to the projectile flux and target thickness. Taking into account the quoted uncertainties in target thickness and projectile flux and also statistical uncertainties, we found the accuracy in experimental total reaction cross sections to be about 10%. The respective numbers are also listed in Table II.

The definition of experimental total reaction cross section is an operational one. The definition is internally consistent with its definition in the framework of the Fresnel-type analysis in the preceding section: Inelastic two-pronged events have been separated from the elastic events with only limited resolution. It is thus obvious that the "elastic" cross section may contain contributions from inelastic two-pronged events. These events will not be accounted for in the reaction cross section. Very important are low-lying Coulomb excitation modes of projectile and target.[26] Also, some very weakly damped reaction products might contaminate the elastic cross section and are thus missing in the total inelastic reaction cross section.

This inherent uncertainty regarding insufficient resolution of elastic and inelastic two-pronged events is unavoidable in the SSNTD method. On the other hand, inelastic scattering with energy loss exceeding the fission barrier of the uranium projectile and of uraniumlike primary reaction products will predominantly lead to fission and at least three prongs will be seen from the interaction. In fact, multiple particle exit states are the dominant reaction channels for the heavy masses and fairly large energies as in the present investigation. It is thus expected that the analysis of the type discussed above will not result in any significant error for the determination of the total inelastic reaction cross section.

C. Comparison with model calculations

In order to compare our inelastic experimental cross sections with model predictions we calculate inelastic reaction cross sections with the optical model and a sharp cutoff approximation.

The optical model (OM) calculations are performed with a program employing a potential of the form

$$V = V_{\text{Coulomb}} + V_{\text{centrifugal}} + V_{\text{nuclear}}$$

TABLE II. Reaction cross sections deduced from elastic ($\sigma_{R,\text{el}}$) and inelastic ($\sigma_{R,\text{el}}$) events in comparison to values from optical model ($\sigma_{R,\text{OM}}$) and sharp cutoff model ($\sigma_{R,\text{SCO}}$) calculations.

Cross section target	$\sigma_{R,\text{el}}$ (mb)	$\sigma_{R,\text{inel}}$ (mb)	$\sigma_{R,\text{OM}}$ (mb)	$\sigma_{R,\text{SCO}}$ (mb)
^{165}Ho	2970[a]	3020±320	3220	3360
^{197}Au	2900[a]	2970±305	3200	3320
^{209}Bi	2780[a]	2940±302	3210	3320

[a]Average of GFM and PSM.

where the nuclear potential follows a Woods-Saxon shape parametrization. Potential parameters are taken as determined by Thomas[27] except for the nuclear radius constant which is empirically set to $r_0 = 1.28$ fm. As we just want to compare inelastic reaction cross sections from experiment with model calculations, refinements to the nuclear potential description are deemed to be unnecessary. A sophisticated OM analysis of the measured data is beyond the scope of this paper.

Sharp cutoff (SCO) cross sections for given c.m. energy E are calculated as

$$\sigma_{SCO} = 10\pi r_b^2 (1 - B/E) \text{ mb} , \quad (12)$$

where the interaction radius r_b (in fm) is determined by the sequence (i = projectile, target)

$$r_i/\text{fm} = 1.28 A_i^{1/3} - 0.76 + 0.8/A_i^{1/3} ,$$

$$C_i = r_i(1 - 1/r_i^2) , \quad (13)$$

$$r_b = 0.8425(C_p + C_t) + 4.49 ,$$

and the Coulomb barrier B (in MeV) is proximity corrected as

$$B/\text{MeV} = \frac{Z_p Z_t e^2}{r_b} - 0.1024\gamma \exp\left[\frac{2.7 - \xi}{0.7176}\right] ,$$

$$\gamma = 11.959 \frac{C_p C_t}{C_p + C_t} \left[1 - 1.7826 \left[1 - 2\frac{Z_p + Z_t}{A_p + A_t}\right]^2\right] , \quad (14)$$

$$\xi = 4.49 - 0.1575(C_p + C_t) .$$

The latter representations are taken from Myers[28] and Blocki et al.[29]

Reaction cross sections calculated according to the above models and compared with the (direct) experimental values are listed in Table II. The model calculated reaction cross sections agree fairly well among each other. However, the experimentally determined elastic and inelastic reaction cross sections seem to underestimate the model values in a systematic way. In all cases, the experimental cross sections are in internal agreement but $\approx 10\%$ below the models. The reason for this discrepancy might possibly stem from problems inherent to the low-resolution analysis and to particular features of the 2π-analysis procedure used in SSNTD work: When evaluating elastic tracks, one is concerned with two-prong events whose track lengths and opening angles obey Eqs. (1) and (2) for projectile and target. It is known,[26,30-35] however, that a certain fraction (at ca. $60 \pm 15\%$) of quasielastic uraniumlike reaction products do not fission. These products are formed in very weakly damped reactions and thus in their kinematics very much resemble elastic products. This contamination of the elastic channel with weakly inelastic products leads to an overestimate of $\theta_{1/4}$ and consequently an underestimate of Λ and σ_{el}. The same events in turn are not counted as inelastic interactions thus diminishing the experimental inelastic cross section σ_{inel} as well. Due to the limited small scattering angle resolution of the SSNTD method, these uncertainties remain unavoidable. Based on the reasonable agreement of the reaction cross sections from the analysis of the elastic and in-

elastic data and from the different models, however, it can fairly be stated that SSNTD data are useful at least for an approximate determination of these quantities. On the other hand, it is also obvious that questions of differences between the optical model, Fresnel analysis, and parametrized S-matrix method or questions of the degree as to which quasielastic events exhibit a binary exit channel cannot be resolved by the present method.

However, a correction of total inelastic cross sections for the abundance of the binary exit channel for uranium-like products in quasielastic reactions is feasible on the basis of model calculations[36] and experimental data.[30-35]

IV. CONCLUSIONS

The experimental data on the elastic scattering of ^{238}U ions by ^{165}Ho, ^{197}Au, and ^{209}Bi are analyzed using the generalized Fresnel model and the parametrized S-matrix method in order to obtain reaction parameters such as interaction radius parameters, grazing angular momenta, and total reaction cross sections. Both analyses produce quite similar results. Improved fits to the data around the quarter point angle are obtained when the l-space window parameter Δ is given a value higher than zero, i.e., the reactions do not proceed in a purely quantal regime. At the present level of accuracy, the experimental data do not indicate variations of the interaction radius parameter with target-projectile combination or with energy in the center of mass.

Elastic and inelastic reaction cross sections obtained with SSNTD agree well for all the systems. The values, however, are systematically low in comparison to optical model and sharp cutoff model calculations. This discrepancy is due to inherent limitations of the 2π-geometry technique and low-energy resolution of SSNTD. As far as the finite solid angle is concerned, this difficulty is overcome by inverted kinematics (i.e., the heavier partner is the projectile) and high bombarding energies. Problems with insufficient separation of elastic and inelastic two-pronged events may diminish with vanishing contributions of the two-particle exit channel in reactions with very fissile ions at fairly large energies.

The presently obtained results indicate that in spite of the simplicity of this low-cost technique, its application yields consistent results and the interaction parameters of heavy ion collisions with heavy targets can be obtained. The applicability of the technique, however, is restricted to experiments with inverted kinematics and with one very fissile reaction partner. We hope that surveys can be extended to other target-projectile combinations at a variety of bombarding energies.

[1]V. Oberacker, H. Holm, and W. Scheid, Phys. Rev. C 10, 1917 (1974).

[2]H. Diehl and W. Greiner, Nucl. Phys. A229, 29 (1974).

[3]H. H. Deubler and K. Dietrich, Phys. Lett. 62B, 369 (1976).

[4]P. A. Gottschalk, G. Grawert, P. Vater, and R. Brandt, Phys. Rev. C 27, 2703 (1983).

[5]P. Glässel, D. v. Harrach, H. J. Specht, and L. Grodzins, Z. Phys. A 310, 189 (1983).

[6]W. U. Schröder and J. R. Huizenga, Treatise on Heavy-Ion Science, edited by D. A. Bromley (Plenum, New York, 1984), Vol. 2, Chap. 3.

[7]S. G. Thompson, L. G. Moretto, R. C. Jared, R. P. Babinet, J. Galin, M. M. Fowler, R. C. Gatti, and J. B. Hunter, Phys. Scr. 10A, 36 (1974).

[8]R. Vandenbosch, M. P. Webb, T. D. Thomas, S. W. Yates, and A. M. Friedman, Phys. Rev. C 13, 1893 (1976).

[9]J. R. Birkelund, J. R. Huizenga, H. Freiesleben, K. L. Wolf, J. P. Unik, and V. E. Viola, Jr., Phys. Rev. C 13, 133 (1976).

[10]J. M. Alexander, H. Delagrange, and A. Fleury, Phys. Rev. C 12, 149 (1975).

[11]G. R. Satchler, Phys. Rev. Lett. 55B, 167 (1975).

[12]M. Lefort, C. Ngô, J. Péter, and B. Tamain, Nucl. Phys. A197, 485 (1972).

[13]H. L. Reynolds, E. Goldberg, and D. D. Kerlee, Phys. Rev. 119, 2009 (1960).

[14]P. W. Riesenfeldt and T. D. Thomas, Phys. Rev. C 2, 711 (1970).

[15]J. J. H. Menet, E. E. Gross, J. J. Malanify, and A. Zucker, Phys. Rev. C 4, 1114 (1971).

[16]W. E. Frahn and R. H. Venter, Ann. Phys. (N.Y.) 24, 243 (1963).

[17]P. Colombani, J. C. Jacmart, N. Poffé, M. Riou, C. Stéphan, and J. Tys, Phys. Lett. 42B, 197 (1972).

[18]W. E. Frahn, Phys. Rev. Lett. 26, 568 (1971).

[19]W. E. Frahn, Nucl. Phys. 75, 577 (1966).

[20]J. S. Blair, Phys. Rev. 95, 1218 (1954).

[21]R. Brandt, P. A. Gottschalk, and P. Vater, Nucl. Instrum. Methods 173, 111 (1980).

[22]P. Vater, H. J. Becker, R. Brandt, and H. Freiesleben, Nucl. Instrum. Methods 147, 271 (1977).

[23]W. E. Frahn, Nucl. Phys. A302, 267 (1978).

[24]J. A. McIntyre, K. H. Wang, and L. C. Becker, Phys. Rev. 117, 1337 (1960).

[25]J. B. Marion and F. C. Young, Nuclear Reaction Analysis (North-Holland, Amsterdam, 1968), Table 5.

[26]W. E. Frahn, Nucl. Phys. A302, 301 (1978).

[27]T. D. Thomas, Phys. Rev. 116, 703 (1959).

[28]W. D. Myers, Nucl. Phys. A204, 465 (1973).

[29]J. Blocki, J. Randrup, W. J. Swiatecki, and C. F. Tsang, Ann. Phys. (N.Y.) 105, 427 (1977).

[30]U. Reus, A. M. Habbestad Wätzig, R. A. Esterlund, P. Patzelt, and I. S. Grant, Phys. Rev. Lett. 39, 171 (1977).

[31]J. V. Kratz, J. O. Liljenzin, A. E. Norris, and G. T. Seaborg, Phys. Rev. C 13, 2347 (1976).

[32]J. V. Kratz, A. E. Norris, and G. T. Seaborg, Phys. Rev. Lett. 33, 502 (1974).

[33]A. Rox (unpublished).

[34]M. Schädel, J. V. Kratz, H. Ahrens, W. Brüchle, G. Franz, H. Gäggeler, I. Warnecke, G. Wirth, G. Herrmann, N. Trautmann, and M. Weis, Phys. Rev. Lett. 41, 469 (1978).

[35]R. J. Otto, M. M. Fowler, D. Lee, and G. T. Seaborg, Phys. Rev. Lett. 36, 135 (1976).

[36]U. Brosa and W. Westmeier, Nucl. Phys. A441, 109 (1985).